

# 1 **Boundary layer structure characteristics under objective** 2 **classification of persistent pollution weather types in the Beijing area**

3

4 Zhaobin Sun<sup>1</sup>, Xiujuan Zhao\*<sup>1</sup>, Ziming Li<sup>1</sup>, Guiqian Tang<sup>3</sup>, Shiguang Miao<sup>1</sup>

5 1. Institute of Urban Meteorology, China Meteorological Administration, Beijing 100089, China

6 2. Environmental Meteorology Forecast Center of Beijing-Tianjin-Hebei, Beijing 100089, China

7 3. State Key Laboratory of Atmospheric Boundary Layer Physics and Atmospheric Chemistry, Institute of Atmospheric

8 Physics, Chinese Academy of Sciences, Beijing 102300, China

9 *Correspondence to:* Xiujuan Zhao(xjzhao@ium.cn)

10

11 **Abstract.** Different types of pollution boundary layer structures form via the coupling of different synoptic systems and  
12 local mesoscale circulation in the boundary layer; this coupling contributes toward the formation and continuation of haze  
13 pollution. In this study, we objectively classify the 32 heavy haze pollution events using integrated meteorological and  
14 environmental data and ERA-Interim analysis data based on the rotated empirical orthogonal function method. The  
15 thermodynamic and dynamic structures of the boundary layer for different pollution weather types are synthesized, and the  
16 corresponding three-dimensional boundary layer conceptual models for haze pollution are constructed. The results show that  
17 four weather types mainly influence haze pollution events in the Beijing area: (a) type1: southerly transport, (b) type2:  
18 easterly convergence, (c) type3: sinking compression, and (d) type4: local accumulation. The explained variance in the four  
19 pollution weather types are 43.69%(type1), 33.68% (type2), 16.51%(type3), and 3.92% (type4). In persistent haze pollution  
20 events, type1 and type2 surpass 80% on the first and second days, while the other types are present alternately in later  
21 stages. The atmospheric structures of type1, type2, and type3 have typical baroclinic characteristics at mid-high latitudes,  
22 indicating that the accumulation and transport of pollutants in the boundary layer is affected by coupled structures in  
23 synoptic-scale systems and local circulation. The atmospheric structure of type4 has typical barotropic characteristics,  
24 indicating that the accumulation and transport of pollutants is primarily affected by local circulation. In type1, southerly  
25 winds with a specific thickness and intensity prevail in the boundary layer, which is favorable for the accumulation of  
26 pollutants in plain areas along the Yan and Taihang Mountains, whereas haze pollution levels in other areas are relatively  
27 low. Due to the interaction between weak easterly winds and the western mountains, pollutants accumulate mainly in the  
28 plain areas along the Taihang Mountains in type2. The atmospheric vertical structure is not conducive to upward pollutant  
29 diffusion. In type3, the heights of the inversion and boundary layers are the lowest due to a weak sinking motion while  
30 relative humidity is the highest among the four types. The atmosphere has a small capacity for pollutant dispersion and is

31 favorable to particulate matter hygroscopic growth; as a result, the type-1 has the highest  $PM_{2.5}$  concentration. In type-4, the  
32 boundary layer is the highest among the four types, the relative humidity is the lowest, and the  $PM_{2.5}$  concentration is  
33 relatively lower under the influence of local mountain–plain winds. The findings of this study allow us to understand the  
34 inherent difference among heavy pollution boundary layers; in addition, they reveal the formation mechanism of haze  
35 pollution from an integrated synoptic scale and boundary layer structure perspective. We also provide scientific support for  
36 the scientific reduction of emissions and air quality prediction in the Beijing-Tianjin-Hebei region of China.

## 37 1 Introduction

38 Over the past 40 years, rapid industrialization and urbanization have caused serious haze pollution problems in China.  
39 Pollutants not only affect the climate system but also reduce visibility, affect city operation, and have a significant negative  
40 impact on human health. Haze pollution creates health costs for residents (Dockery et al., 1993; McDonnell et al., 2000) and  
41 emissions reductions costs (D'Elia et al., 2009). Governments must play a more flexible role and adopt an optimized strategy  
42 between health costs and emissions costs based on national or local economic affordability to reduce emissions (Lee et al.,  
43 2016). From an operability perspective, the timings of different emissions reductions strategies are largely dependent on  
44 trends in atmospheric pollution dispersion conditions (Zhai et al., 2016). Haze pollution is the combined effect that excessive  
45 emissions and adverse meteorological conditions have on the dispersion of pollutants (He et al., 2013; Li et al., 2017). With  
46 relatively few changes in the emission source, the diffusion conditions largely determine the duration and pollution level of a  
47 haze event.

48 First, from an atmospheric circulation perspective, persistent haze pollution generally corresponds to persistent adverse  
49 meteorological conditions for pollutant dispersion (Zheng et al., 2015), where persistent anomalies in atmospheric  
50 circulation are an important background (Wang et al., 2015). These conditions cause stabilized vertical stratification and low  
51 horizontal wind speeds (Chamorro et al., 2010; Park et al., 2014), such that the combination of these two conditions form  
52 "calm weather." From a large-scale climate circulation perspective (Markakis et al., 2017; Zou et al., 2017), previous studies  
53 have suggested that, if global warming trends continue, the probability of adverse atmospheric pollutant dispersion will  
54 continue to increase (Cai et al., 2017). Where the reduction in sea ice can lead to the weakening of the Rossby wave activity  
55 south of 40°N, rendering the lower layer colder and a reduced moisture content, a stable atmosphere, weaker wind speeds,  
56 and an increased chance of heavy haze pollution (Wang et al., 2015; Chen et al., 2015). These results show that the troposphere  
57 in the Beijing-Tianjin-Hebei area can produce a continuous deep downdraft under flat circulation or a weak high-pressure  
58 system, along with the boundary layer's southerly wind yielding the temperature inversion height and decrease in the  
59 atmospheric capacity, which provides a favorable dynamic condition for the maintenance and aggravation of haze pollution  
60 (Wu et al., 2017). Zhang et al. (2016) use the Kirchhofer technique to classify the circulation patterns, examining the  
61 influence that the monsoon has on the occurrence frequency of different weather patterns and air quality.

62 Second, the pollutant concentration also depends on local mesoscale circulation coupled with a stable boundary layer and  
63 synoptic-scale system (Miao et al., 2017), for example, valley wind, sea–land wind, heat island circulation, and mountain–  
64 plain wind. Even under conditions associated with weaker synoptic scales, these mesoscale systems largely determine the  
65 peak concentration and spatial-temporal distribution of the pollutants (Miao et al., 2017; Li et al., 2019). Previous studies  
66 have examined the interaction between aerosols and the boundary layer (Wu et al., 2019; Zhong et al., 2018; Wang et al.,  
67 2018a; Wang et al., 2018b; Zhou et al., 2018). Ding et al. (2016) find that black carbon aerosols play a key role in reducing  
68 the height of the boundary layer and enhancing haze pollution. Huang et al. (2018) investigate the interaction between  
69 aerosols and the boundary layer in North China using long-term observational data, quantifying the contribution of aerosols  
70 to the heating of the top layer of the boundary layer and cooling of the surface layer.

71 In summary, previous studies have achieved results in the study of the influence that the weather system and boundary layer  
72 have on the concentration of aerosols. A comprehensive analysis of these two aspects, that is, combining weather  
73 systems and the structure of the boundary layer, however, is still rare. Liao et al. (2018) use the Self-Organizing Map method  
74 to classify the boundary layer in the Beijing area, as well as to examine the relationship between the classification results  
75 and pollutant concentrations. Miao et al. (2017) and Xu et al. (2019) use the obliquely rotated principal component analysis  
76 in T-mode (T-PCA) approach to classify synoptic patterns, analyzing the structure of the boundary layer and concentration  
77 of surface pollutants under different weather types in summer. The Beijing area is located in the transition zone between the  
78 plain and mountainous areas, with mountains to the west, north, and east. The southeastern region of Beijing is a flat plain  
79 that slopes toward the Bohai Sea. More than 20 million people live in Beijing who are affected by both the weather system  
80 and local circulation in the boundary layer. To formulate optimized emissions reduction strategies, we must master the main  
81 control factors that affect the haze pollution diffusion conditions in Beijing under different weather and boundary layer  
82 conditions. At present, under the influence of different haze pollution weather types, there are still a lack of studies on the  
83 three-dimensional haze pollution structure of the boundary layer, especially as the structure of the heavy haze pollution  
84 boundary layer is not entirely identical. The above-mentioned weather classification methods do not take into account the  
85 continuity of the one haze pollution event, such as the first day of pollution weather pattern is same as the second day? what  
86 is the difference in the structure of the boundary layer between haze pollution weather types? The different structures of the  
87 boundary layer correspond to the different accumulation characteristics and pollutant efficiencies. However, previous studies  
88 did not unravel structure differences of the heavy haze pollution boundary layer. Based on the objective classification of the  
89 pollution weather types, we examine the boundary layer structures of different pollution synoptic types, revealing that the  
90 thermal and dynamic mechanisms of the boundary layer structures inhibit the diffusion of atmospheric pollutants. Based on  
91 the two interrelated dimensions, that is, the weather system and boundary layer structure, we systematically investigate the  
92 meteorological mechanism of haze pollution formation.

93

## 94 **2Data and methods**

### 95 **2.1 Meteorological data**

96 The weather classification data were derived from the ERA-Interim data from 2014–2017. ERA-Interim (0.125 °×0.125 °) is a  
97 new reanalysis data from the ECMWF (European Centre for Medium-Range Weather Forecasts ) after the ERA40, with 60  
98 vertical layers and partially overlaps with the ERA40 in time. However, significant progress has been made in data  
99 processing, for example, from the three-dimensional assimilation system(3-D VAR) to the four-dimensional assimilation  
100 system(4-D VAR).The model parameters were changed and the horizontal resolution was enhanced with the use of more  
101 satellite and ground-based observations(<https://apps.ecmwf.int/datasets/>).

102 The 850hPa geopotential height field (30–50 °N, 110–128 °E) of the ERA-Interim was used to classify the weather system.  
103 The meteorological elements at 850hPa interact with the meteorological elements in the boundary layer. At the same time,  
104 the 850hPa is evidently influenced by the free atmosphere, especially in Beijing area, which can be regarded as the transition  
105 layer between local thermal circulation (valley wind, sea–land wind, and mountain–plain wind ) and the free atmosphere. In  
106 addition, the hourly relative humidity, visibility, and wind speed observed at the Beijing Observatory (39.93 °N, 116.28 °E)  
107 were used in this study.

108 A 12-channel (5water channels and 7oxygen channels) microwave radiometer (Radiometrics, Romeoville, IL, U.S.A.) was  
109 used to measure the relative humidity and temperature profile in the atmosphere. The microwave radiometer was installed in  
110 the Beijing Observatory (39.93 °N, 116.28 °E) and was calibrated every three months. The wind profiles, including the wind  
111 speed and direction between 100 and 5,000m, are measured at the same station by a wind profiler. The wind profiler radar  
112 provides a set of profile data every 6min at a detection height of ~12–16km.

### 113 **2.2 Air quality monitoring data and haze pollution event definition**

114 Hourly PM<sub>2.5</sub> concentrations at 12 national stations and the daily air quality index (AQI)in Beijing are available from  
115 <http://zx.bjmemc.com.cn/?timestamp=1564483254009>. Surface PM<sub>2.5</sub> mass concentrations were measured by the tapered  
116 element oscillating microbalance method. The measurements were calibrated and quality controlled according to the Chinese  
117 environmental protection standard (HJ 618-2011).

118 As this study focuses on episodes of heavy haze pollution, we first defined the criteria. Haze is defined by the relative  
119 humidity and visibility; therefore, the haze pollution level is defined by the AQI and the primary pollutant. Considering that  
120 haze pollution mainly refers to reduced visibility caused by fine particulate matter, as well as taking into account the effects  
121 of the pollution levels and duration, the screening criteria for heavy haze pollution were still based on the AQI, PM<sub>2.5</sub>  
122 concentration, and the duration of low visibility. The specific criteria of a haze pollution event can be defined as follows: the  
123 AQI reaches a moderate pollution level (AQI≥150) for more than or equal to 3 days and at least 1 day reaches the heavy  
124 pollution level (AQI>200). The primary pollutant is PM<sub>2.5</sub> in Beijing area. As defined by the AQI, the 24-h average  
125 concentration of PM<sub>2.5</sub> must be above 115 μg m<sup>-3</sup> for more than three consecutive days and above 150 μg m<sup>-3</sup> for at least 1

126 day. At the same time, the accumulated time of horizontal visibility, that is, less than 5 km, has a duration of at least 12 h  
127 each day at the Beijing Observatory station.

128 Based on these criteria, 32 events (125 days) were screened for heavy haze pollution in Beijing between 2014 and 2016.  
129 Eight events occurred in spring and summer while 24 events were concentrated in autumn and winter, 32 events accounting  
130 for 75% of the events that occurred during the study period (2014–2016). We collected ground-based routine meteorological  
131 observation data in North China, L-band radar second-order sounding data (including wind, temperature, and humidity),  
132 wind profile data, ceilometer data, and tower data during these events.

### 133 **2.3 Attenuated backscattering coefficient measurements and boundary layer height calculation**

#### 134 **2.3.1 Attenuated backscattering coefficient measurements**

135 We used the CL31 and CL51 Vaisala-enhanced single-lens ceilometer instrument, which uses the pulse diode laser LIDAR  
136 (laser detection and ranging) technology to measure the backscattering profile of atmospheric particles and the cloud height.  
137 The main parameters of the CL31 and CL51 are respectively as follows: range of 7.6 and 13 km, reporting periods of 2–120  
138 and 6–120s, reporting accuracy of 5 and 10 m/33 ft, peak power of 310 W, and wavelength of 910 nm. The geographic location  
139 of the station is 39.974° N and 116.372° E, with an elevation of approximately 60 m (Tang et al., 2016).

#### 140 **2.3.2 Boundary layer height calculation**

141 As the lifetime of a particle is long, that is, several days or weeks, the particle concentration distribution in the boundary  
142 layer is more uniform than that of the gaseous pollutant, whereas the particle concentration in the boundary layer is  
143 significantly different from that in the free atmosphere. By analyzing the backscattering profile of the atmospheric particles,  
144 we located the abrupt change in backscattering at the top of the boundary layer.

145 This study used the gradient method (Christoph et al., 2007; Zhang et al., 2013; Tang et al., 2015) to determine the boundary  
146 layer heights. The maximum negative gradient in the aerosol backscattering coefficient profile occurs at the top of the  
147 boundary layer, but is easily disturbed by data noise and the aerosol structure. Therefore, we must select a continuous region  
148 of time or space for averaging to smooth the contour map vertically after averaging and adopt an improved gradient  
149 ([http://isars2010.uvsq.fr/images/stories/posterabstracts/p\\_bls06\\_muenkel.pdf](http://isars2010.uvsq.fr/images/stories/posterabstracts/p_bls06_muenkel.pdf)) method to manage severe weather (such as  
150 precipitation and fog). Despite this, the gradient method still has certain defects, especially for neutral atmospheric  
151 stratification, where the inverse calculation of the boundary layer height is not accurate.

### 152 **2.4 Objective classification of pollution weather types**

153 Using the ERA-Interim reanalysis data, the 925 hPa geopotential heights of all pollution events in this study were analyzed  
154 with the rotated empirical orthogonal function (REOF) to determine which mode the pollution events belong to according to  
155 the characteristic values of the different pollution events for determining the days characterized by specific types of pollution

156 weather the empirical orthogonal function (EOF) analysis, the first few main components are the focus of the analysis  
157 element variance, such that the EOF method can highlight the entire correlation structure of the analysis element. However,  
158 the local correlation structure is not sufficient, which is a defect of the pollution weather classification based on the EOF.  
159 Based on the EOF analysis, the REOF transforms the load characteristic vector field into a maximum rotation variance, as a  
160 result of which each point in the rotation space vector field is only highly correlated with one or a few rotation time  
161 coefficients. Thus, the high load value areas are concentrated in smaller areas, while the remaining areas are relatively small  
162 and nearly 0, highlighting the pattern and characteristics of the abnormal distribution of elements (Paegle et al., 2002; Chen  
163 et al., 2003), the classification of heavy pollution weather types based on this method is more consistent with the  
164 requirements of this study. Pollution weather types were classified by the REOF method to analyze the differences in the  
165 structures of the pollution boundary layer.

## 166 **3 Results and discussion**

### 167 **3.1 Pollution weather type classification and horizontal characteristic analysis**

168 In this study, the 925hPa geopotential height is used to classify the pollution weather types into four categories with the  
169 REOF method, as shown in Fig. 1: (a) type1, that is, influenced by southerly winds at the rear of the high pressure system, (b)  
170 type2, that is, influenced by easterly winds at the bottom of the high pressure system, (c) type3, that is, a weak downdraft  
171 effect in the high pressure system, and (d) type4: no significant weather system. In this study, we observed 125 days of  
172 heavy polluted weather. Among these days, type1, type2, type3, and type4 had 67, 27, 21, and 10 days, respectively (Fig.2),  
173 where the four weather types accounted for 53.6, 21.6, 16.8, and 8.0% of the total sampled weather event days, respectively.  
174 The total interpretation variance of the four types for all events was 97.8% while the independent interpretation variance was  
175 43.69, 33.68, 16.51, and 3.92%, respectively (Fig. 2) is indicates that an objective weather classification can effectively  
176 obtain the main feature information of the pollution weather types.

177 shown in Fig. the Beijing area is located toward west of the high-pressure system that has its center located in the sea.  
178 The low pressure system is located in the northern Hebei province for type1, where southerly winds control the 925hPa,  
179 which is favorable for the regional transportation of pollutants. When type2 appears, the Beijing area is located at the bottom  
180 of the high pressure system in Northeast or North China. In the plain area, the sea level pressure in the eastern part of Beijing  
181 is higher than that in the central Beijing area, such that there is an evident pressure gradient. Due to pressure-gradient forcing,  
182 the boundary layer appears within the easterly wind component while the easterly wind speed is smaller, which leads to  
183 pollutant convergence into the plains along the Taihang Mountains, When type3 appears, the high pressure center was  
184 located in the middle of Mongolia, where Beijing was in the front of the weak high pressure system, with a northwest current  
185 at 925hPa(Fig. 1) however, the wind speed was lower than that affected by strong cold air, because of which it was  
186 difficult to penetrate the lower layer of the boundary layer and the wind can only exist in the upper atmosphere of the  
187 boundary layer. When type4 appears, the center of the high pressure system is located further to the north in the western part

188 of Mongolia and southern Hebei province. Here there is only a low pressure system with a smaller spatial and temporal  
189 scale. On the other hand, the synoptic-scale low pressure system is already located over the sea in the eastern Jianghuai  
190 region, showing that the high and low pressures corresponding to the synoptic-scale system are far from the Beijing area,  
191 which results in a smaller synoptic-scale pressure gradient in Beijing and the surrounding areas (Fig. 11). Most areas in North  
192 China do not have strong weather systems and the average wind speed of the boundary layer is smaller, which is favorable to  
193 the formation and maintenance of the local circulation considering the topography in the Beijing area. The wind speed of  
194 type4 is more difficult to determine via the evolution of the wind field in the lower boundary layer based on the effect of  
195 descending momentum. Therefore, the dynamic pollutant process in the boundary layer in type4 is more related to the local  
196 circulation.

### 197 3.2 Vertical thermal and dynamic structure characteristics under four weather types

198 Figure 3 shows that the strong inversion is located at 800–900hPa for type1. In type2, easterly winds with low temperatures  
199 influence the temperatures below 800hPa, where a cooling layer appears at 900 hPa, with the height of inversion between  
200 700 and 800hPa. The inversion height for type3 is the lowest among the four types due to the sinking motion, where the  
201 inversion is mainly below 900hPa, which causes a rapid decline in the atmospheric capacity. The atmospheric structure is  
202 also relatively stable in type4, whose inversion structure is similar to type2. The mechanism of the thermal structure, however,  
203 is different. Here the inversion height of this type is between 700 and 800hPa.  
204 As shown in Fig. 4, the basic flow is the southerly wind below 2,000m in type1, where a southwest wind appears from 500–  
205 2,000m. The southerly wind is below 500m between 04:00 and 20:00 and the easterly wind appears at other times. The  
206 southerly wind speed at 500m is strong, while the easterly wind is weak. In type2, the basic flow above 1,000m is westerly  
207 wind, where the layer between 500 and 1,000m is a weak wind layer. We note that the wind velocity in this layer is the  
208 smallest when there is an increase in the easterly component below 500m. This indicates that the weak wind layer is the wind  
209 shear transition layer between the westerly wind above 500m and the easterly wind below 500m. The easterly and westerly  
210 winds cancel each other at this height and form a small wind velocity layer. From 04:00 to 20:00, southerly winds appear  
211 below 500m while we observe the appearance of easterly winds at other times. The space-time structure of the wind field  
212 below 500 m was similar to that of type1, but the southerly wind speed was lower than in case of type1. In type3, the wind  
213 above 500m originates from the northwest from 04:00 to 14:00. At altitudes below 500 m, the wind is southerly and  
214 northerly at other times. Whether it is southerly or northerly, the wind speed is smaller. Mountain–plain wind in the Beijing  
215 area causes this diurnal and nocturnal circulation of the wind field. In type3, the wind velocity below 500m is less than that  
216 of type1 and type2, because the basic flow is northerly, where northerly wind superposes onto the plain wind (southerly),  
217 which may weaken the southerly wind speed. The observed data are the superposition results of two scale wind fields (i.e.  
218 local circulation and basic flow). Westerly or weak northerly winds above 1,000m in type4 control the atmosphere, where  
219 the wind velocity below 1,000m is significantly weak. For the majority of the time, the wind velocity is less than  $4 \text{ m s}^{-1}$ , but  
220 the mountain–plain diurnal cycle wind can still be observed from the diurnal variation in the wind direction. From 08:00 to

221 18:00, the wind is southerly while mainly northerly at night. Weak wind speeds last for a long period in the boundary layer  
222 of type4, because of which the local thermal and dynamic conditions can become the main factors that affect the spatial-  
223 temporal distribution of haze pollutants in Beijing.

224 Figure shows that, below 700hPa, type1, type2, and type4 are ascending movements. The maximum of the synoptic scale  
225 ascending movement appears in 900–950hPa. With an increase in the height, the intensity of the ascending movement  
226 gradually weakens, whereas in type3, below 750hPa can be characterized as a sinking movement. The intensity of the  
227 sinking movement increases gradually with decreasing height where the maximum of the sinking movement appears at 900–  
228 950hPa. The intensity of the subsidence movement from this layer at 900–950hPa to the ground decreases a second time.  
229 Therefore, the sinking movement affects the inversion layer of type3, where the height of the inversion layer is the lowest of  
230 all types, resulting in type3 characterized by the smallest humidity among the four types.

231 Based on Fig. the relative humidity profiles for the four weather types have both similarities and differences in their space-  
232 time structures. The similarities in the four types are the increased and decreased relative humidity below 1,000m during the  
233 night and day, respectively, with a reverse in the relative humidity layer appearing during the day. The relative humidity of  
234 the surface layer decreases daily from 10:00 to 20:00 with an increase in the solar radiation. The thickness of the dry layer in  
235 the surface layer increases continuously, reaching its maximum height at ca. 14:00 or 15:00 every day, but the maximum  
236 height of the dry layer does not exceed 500m. The top of the dry layer is the reverse of the relative humidity layer. Above  
237 1,000m, the relative humidity of the other three types, except type2, decreases significantly during the day.  
238 The difference in the relative humidity field among the four types can be summarized as follows. The average relative  
239 humidity below 1,000m is higher than that above 1,000m. The inverse relative humidity structure appears below 500m in  
240 type2 and type3 from 00:00 to 05:00, with a maximum relative humidity center of more than 90%. Above 500m, the relative  
241 humidity also increases from 05:00 to 12:00. The relative humidity structures of type1, type2, and type3 all contain a  
242 baroclinic structure from lower to higher levels, where the baroclinic structure in type2 is more evident because the basic  
243 flow in type2 is westerly, which reflects the baroclinic characteristics of the atmosphere in the mid-high latitudes of East  
244 Asia. The basic flow is generally westerly in this area, where type1 and type3 are more typical of the disturbances in the  
245 northerly and southerly wind in the westerlies, which is the fluctuation feature of the basic flow. The relative humidity  
246 profile in the pollution boundary layer formed under the condition of wave-current interaction in the atmosphere (Fig. 6)  
247 Type2 has strong westerly characteristics (Fig. 4) which reflects more baroclinic characteristics in the atmospheric vertical  
248 structure for the westerlies. Based on the analysis of the wind field, type4 is characterized by an average wind speed that is  
249 the weakest among the four types. Three important factors determine the baroclinicity, that is, the density gradient, pressure  
250 gradient, intersection angle between the density surface and pressure surface. This may be an important factor why relative  
251 humidity field has more barotropic characteristics. From the analysis of the baroclinic and barotropic characteristics, we can  
252 observe that the weather systems of type1, type2, and type 3 have a significant influence on the accumulation and transport  
253 of pollutants in the Beijing area. The mountain–plain wind in type4 can occur due to weakening in the weather system (Fig.  
254 4).



### 255 3.3 Construction of 3-D conceptual model for the pollution boundary layer

256 Based on the characteristics of the circulation field and the vertical thermodynamic structure for the four weather types, we  
257 established conceptual models of the boundary layer structure under the influence of the four pollution weather types is  
258 established, which are: (a) type1: southerly transport; (b) type2: easterly convergence; (c) type3: sinking compression; (d)  
259 type4: local accumulation (Fig. 4). When type 1 appears, the Beijing area is located at the rear of the high-pressure system,  
260 consistent with southerly winds throughout the atmosphere and multilayer inversion occurs in the boundary layer. Under the  
261 influence of a southerly wind, haze pollutants accumulate in front of the Yan and Taihang Mountains. The air pollutants in  
262 the Hebei region have evident regional transport features. When type2 appears, the Beijing area is located at the bottom of  
263 the high-pressure system, where the air above 850hPa has a westerly wind, with easterly winds below 850hPa. Under the  
264 influence of easterly winds below 850hPa, haze pollutants tend to accumulate in front of the Taihang Mountains. The cross-  
265 mountain air mass flows from west to east, preventing the further dispersion of air pollutants in front of the Taihang  
266 Mountains. When type3 appears, a weak high-pressure system controls the Beijing area. A weak subsidence northwest flow  
267 influences the atmosphere above 850hPa, which further compresses the capacity of the atmosphere to absorb pollutants in  
268 the boundary layer. The southerly wind at 850hPa is favorable for pollutant transportation in the region and accumulation in  
269 front of the Yan and Taihang Mountains. The atmospheric vertical structure in the high-level northwest wind and low-level  
270 southward wind provides excellent conditions for the stability of atmospheric stratification with respect to dynamic  
271 conditions and a thermal structure. The 850hPa southerly winds favor regional pollutant transport and their accumulation in  
272 the area along the Yan and Taihang Mountains. The atmospheric vertical structure of the high-level northwest wind and low-  
273 level southerly wind provides excellent conditions for stratification stability in terms of dynamic-thermal structures because  
274 southerly wind at 850hPa is warm advection, where advection inversion can form in the boundary layer, while weak  
275 subsidence above 850hPa can cause subsidence inversion. These two inversion mechanisms are coupled at the interface  
276 between the northwest wind and southerly wind, resulting in stable atmospheric stratification. When type4 appears, there is  
277 often no evident synoptic-scale system surrounding Beijing, with a weak pressure gradient above 850hPa. Therefore, the  
278 average wind speed is weak. The most important local circulation in Beijing, that is, the mountain–plain wind, begins to  
279 form in the boundary layer and plays an important role in the spatial and temporal distribution of atmospheric pollutants,  
280 with the wind direction continuously shifting from the south to the north. The air pollutants accumulate near the terrain  
281 convergence line formed by the mountain–plain wind. The terrain convergence line also swings from north to south, such  
282 that air pollution in the Beijing area often appears as a “different sky” relative to a clean sky in the north and a polluted sky  
283 in the south.

284

### 285 3.4 Effects of the four pollution weather types

#### 286 3.4.1 Statistical analysis: effects of the four weather types on haze pollution

287 Figure 8 shows the statistical characteristics of the  $PM_{2.5}$  concentrations and meteorological elements in terms of the four  
288 polluted weather types. The daily average  $PM_{2.5}$  concentration in type3 is the highest at  $245 \mu g m^{-3}$  and type4 is the lowest at  
289  $181 \mu g m^{-3}$  (Fig. 4). The daily average relative humidity values of the four pollution weather types are  $>60\%$ , with a  
290 maximum relative humidity of 72.3% in type3 and a minimum relative humidity of 63.5% in type4 (Fig. 8b). Under the  
291 influence of a high relative humidity and high  $PM_{2.5}$  concentration, the daily average visibility for the four heavy pollution  
292 weather types is less than 4,000m, with a minimum daily average visibility of 2,193m in type1. The maximum daily average  
293 visibility is 3,624m in type4 (Fig. 8c). The mean 24h wind speeds for the four pollution weather types are all less than  $2.0 m$   
294  $s^{-1}$ .

295 The mean daily wind speeds of type1 and type3 are both smaller, that is,  $1.38$  and  $1.49 m s^{-1}$ , respectively. The mean daily  
296 wind speeds of type2 and type4 are relatively faster, that is,  $1.70$  and  $1.76 m s^{-1}$ , respectively (Fig. 8d). There is a significant  
297 negative correlation between the boundary layer height and  $PM_{2.5}$  concentration. The lowest boundary layer height was  $386.5$   
298 m for type3, followed by type1, whereas type4 had the highest boundary layer height.

299 In this study, we calculated the distribution of the weather types from the first to last day of the persistent haze pollution  
300 events (Fig. 9). The daily synoptic types from the first to eighth day of persistent haze pollution events were calculated. As  
301 the number of pollution events that lasted more than five days is relatively small, the classification results were combined  
302 with the statistics for the events defined as greater than or equal to five days. The results show that the cumulative proportion  
303 of type1 and type2 occurrences on the first and second pollution day are more than 80%, indicating that regional transport  
304 plays a more prominent role in the initial stage of haze pollution formation, which is consistent with previous  
305 analyses (Zhong et al., 2018). On the third day and thereafter, the proportion of type1 began to decrease, but still exceeded  
306 30%. Type2, type3, and type4 began to alternately affect the Beijing area. This indicates that, after the first and second days,  
307 the center of high pressure over East China in type1 began to move eastward away from the mainland. Beijing is located at  
308 the rear of the high-pressure system, where the  $PM_{2.5}$  concentration corresponding to type1 increases throughout most of the  
309 day. The timing of the initial rise in the  $PM_{2.5}$  concentration is the earliest among the four types, which indicates the role of  
310 the rear within the high-pressure system in the transmission of pollutants (Fig. 10a). When the upstream weather system  
311 begins to affect the Beijing area, it is occasionally located at the bottom of the high-pressure system (type2). The diurnal  
312 variation in the  $PM_{2.5}$  concentration in type2 was similar to the mean annual variation in the  $PM_{2.5}$  concentration in the  
313 Beijing area. The first peak was at 10:00 and the second was at 20:00 (Zhao et al., 2009) (Fig. 10a). The weak high-pressure  
314 system in type3 can directly affect the haze pollution diffusion conditions in the Beijing area, but the intensity of the cold air  
315 behind the upper trough is weak. The  $PM_{2.5}$  concentration in type3 is higher at night and lower during the day, with the  
316 highest average  $PM_{2.5}$  concentration among the four types. Based on this analysis, we can observe that, in type3, the height of  
317 the inversion layer is the lowest and the atmospheric capacity to contain pollutants is also the lowest under the influence of a  
318 weak downdraft (Fig. 10a). In type4, there is no evident weather system that affects the Beijing area. An increase in the  
319 thermal difference between the mountain and plain affects local circulation development. The average  $PM_{2.5}$  concentration in  
320 type4 is the lowest among the four types. The diurnal variation in the  $PM_{2.5}$  concentration shows a typical "v" pattern. After

321 sunrise, the  $PM_{2.5}$  concentration begins to decrease while, after sunset, the  $PM_{2.5}$  concentration increases significantly, which  
322 was due to the fluctuation of aerosols under local meteorological conditions (Fig. 10a). Based on Fig. 10b, the boundary  
323 layer height of type3 is the lowest among all types for most part of a day, which is mainly related to the suppression of the  
324 weak synoptic-scale downdraft. The change in the trend of the boundary layer height is similar to that type2 and type4  
325 most of the day. However, the boundary layer height is less developed when the thermal conditions are strongest between  
326 12:00 and 18:00, which is similar to type3. The boundary layer heights of type2 and type4 are relatively high, and the  
327 corresponding  $PM_{2.5}$  concentrations are the lowest out of the four pollution types (Fig. 10b).

328 The above analysis shows that in one persistent multi-day pollution event, the weather patterns that affect the Beijing area  
329 change daily, that is, they also change according to the basic principles of synoptic dynamics, which is the natural  
330 development and evolution of rossby waves in the mid-high latitude westerly belt. This also indicates that it is not  
331 appropriate to classify a multi-day pollution event as a defined type (such as the low-pressure or high-pressure type). We  
332 cannot rule out the possibility that a pollution event may occur for several consecutive days under the influence of a low-  
333 pressure system, which is a rare event. Even then, this may also be a combination of different low-pressure systems. In  
334 addition, we note that, in one persistent multi-day heavy pollution event, different types of pollution weather types are linked  
335 together in a permutation that affects the structure of the boundary layer and thus the change in the  $PM_{2.5}$  concentration (Fig.  
336 9). As different types of weather systems form haze pollution events, we discuss type of boundary layer structure formed  
337 by certain weather systems in the Beijing area and how this boundary layer structure influences the evolution of haze  
338 pollution formation.

### 339 3.4.2 Effects of four weather types on the 3-D spatial-temporal evolution of haze pollution

340 Figure 11 shows aerosol vertical distribution under the influence of the boundary layer structure for the four pollution  
341 weather types. The wind below 2,000m for type1 in Fig. 11 is southerly (Fig. 4), which facilitates regional pollutant transport.  
342 From 10:00 to 11:00, a v-shaped notch appears in the vertical structure of the aerosol at a height of 500–1,000m, which  
343 shows that there is a decrease in the extinction ability of the entire atmosphere below 1,000m. The boundary layer height  
344 rises above 1,000m from 11:00 to 17:00, showing an improvement in the local haze pollutant dispersion condition in Beijing,  
345 but the aerosol below 1,000m increases, which is more evident below 500m. This indicates that extrinsic aerosols are  
346 transported to Beijing area, which is consistent with the transport characteristics of southerly wind in the entire type1  
347 atmosphere. Under the influence of southerly winds, the sensitive source areas related to the Beijing area are generally the  
348 plain areas along the Taihang Mountains in Hebei province (Wang et al., 2017). According to the dynamics, the positive  
349 vorticity advection in the direction of Beijing forms in the plain area. The positive vorticity advection in this boundary layer  
350 has two functions. First, the positive vorticity airflow is affected by the friction, coriolis effect, and pressure-gradient force.  
351 Second, the positive vorticity advection continuously transports the converging space field to the Beijing area and, at the  
352 same time, also transfers a large amount of external pollutants. The above analysis can explain the significant increase in the  
353  $PM_{2.5}$  concentration in the surface layer and the corresponding increase in the number of aerosols within 1,000m, which is a  
354 common phenomenon during regional haze pollution events in Beijing, Hebei, and Tianjin. However, westerly or weak

355 northwest winds occur above 1,000m in type2. The dynamic stratification structure between the upper and lower layers is not  
356 favorable for downward momentum transfer, which results in the strengthening of southwesterly winds in the boundary layer  
357 (Fig. 4). Therefore, after 11:00 in type1, the aerosol in the boundary layer begins to increase while after 12:00 in type2, there  
358 is an increase in the aerosol in the boundary layer shown in Fig. 12. There is a strong southerly wind in type1. Pollutants  
359 concentrate in the plain areas along the Taihang and Yan mountains. The  $PM_{2.5}$  concentration in the eastern part of the  
360 Beijing-Tianjin-Hebei plain was significantly lower than that in the western part along the mountains in type2. Northerly air  
361 flow mainly influences the entire atmosphere (above 500m) of type3 in Fig. 10. In general, the air flow in the atmosphere  
362 indicates the arrival of cold air, which generally corresponds to good diffusion conditions. However, the lower part of the  
363 boundary layer is often associated with a slow wind speed or southerly wind, which indicates that the northerly wind does  
364 not reach the ground. This is an important feature of the type3 boundary layer structure. Weak subsidence caused by the  
365 northerly wind restrains the development of the height of the boundary layer, and as a result, aerosols are confined in the  
366 boundary layer and cannot spread to high altitudes. The near-surface layer is convergent and ascending, where the  
367 convergence of air currents causes the pollutants in the surrounding area to accumulate locally. As shown in Fig. 11, in type3,  
368 the wind speed in the Hebei plain area is relatively low, but the northerly surface wind speed in the western and northern  
369 mountainous areas of the plain is relatively high. This indicates that there is a northerly wind (Fig. 10, type3) in the upper  
370 part of the small wind layer in the Beijing-Tianjin-Hebei plain. The pollutant concentrations in the surface layer of the  
371 Beijing-Tianjin-Hebei plain are higher than those in type1 and type2. The boundary layer height in type4 (Fig. 11) is the  
372 highest among the four types (Figs. 8e and 10). The capacity in the boundary layer for aerosols is larger than that of the  
373 other three types. The wind speed above 1,500m is weaker, the wind direction below 1,500m is westerly, and the wind speed  
374 below 1,500m is smaller, such that there was no significant wind speed in the region, which indicates that there was no  
375 strong weather system in the region. From a wind direction perspective, the wind was southerly during the day and northerly  
376 at night. This is a typical mountain-plain wind in the Beijing area (Fig. 6). With changes in the mountain and plain winds,  
377 there will be a convergence line in the Beijing plain area, which can be occasionally continuous or fractured.

#### 378 **4 Conclusion**

379 In this study, we objectively classified pollution weather events based on the REOF method using integrated observation  
380 data from meteorology and the environment, combined with the ERA-Interim reanalysis data (0.125° × 0.125°). We then  
381 synthesized the thermodynamic and dynamic structures of the boundary layer under the different pollution weather types to  
382 construct the corresponding boundary layer conceptual models. The results show that four weather types mainly affect the  
383 pollution events in Beijing: (a) type1: southerly transport, (b) type2: easterly convergence, (c) type3: sinking compression,  
384 and (d) type4: local accumulation. The explained variance in the four pollution weather types were 43.69% (type1), 33.68  
385 (type2), 16.51% (type3), and 3.92% (type4), respectively.

386 In persistent pollution events, the proportion of type1 and type2 occurrences were more than 80% on the first and second  
387 days, with subsequent alternations in other types. The atmospheric structures of type1, type2, and type3 have typical  
388 baroclinic characteristics in the mid-high latitudes, indicating that synoptic-scale systems, together with local circulation,  
389 affect the accumulation and transport of pollutants in the boundary layer. On the other hand, the atmospheric structures of  
390 type4 have typical barotropic characteristics, which indicates that local circulation plays a major role in pollutant  
391 accumulation and transport. This is the first time that the baroclinic and barotropic characteristics of the atmosphere have  
392 been introduced into the discussion of pollution boundary layer.

393 Among the four types, southerly winds, with certain thicknesses and intensities, appeared in the boundary layer of type1,  
394 which was favorable for the transportation of pollutants to Beijing, accumulating more in areas along the Yan and Taihang  
395 Mountains. On the other hand, the pollution level in the central plain area of Hebei was relatively small. For type2, the  
396 pollutants mainly concentrated along the Taihang Mountains due to the influence of the interaction between weak easterly  
397 winds and topography. The vertical structure of the atmosphere was unfavorable for pollutants to ascend into the mountains.  
398 Type 3 had the lowest inversion height, boundary layer height, and the highest relative surface humidity, which are favorable  
399 for PM<sub>2.5</sub> hygroscopic growth. Finally, type3 had the highest PM<sub>2.5</sub> concentration. Type4 had the highest boundary layer  
400 height and lowest relative humidity among the four pollution types, whose PM<sub>2.5</sub> concentration was relatively low when  
401 exposed to local mountain–plain winds. Pollutant accumulation is related to dynamic oscillation along the convergence line  
402 of the mountain terrain. The results of this study allow us to understand the formation mechanism of different heavy  
403 pollution boundary layers from synoptic scale and boundary layer perspectives, as well as to provide scientific support for  
404 scientific emissions reduction and air quality prediction. The different heavy pollution weather types and heavy pollution  
405 boundary layers not only reflect the interaction between the atmospheric mean flow and fluctuation, but also reflect the  
406 process of heavy pollution weather types shaping the boundary layer. Changes in pollution weather patterns cause the  
407 pollution boundary layer to change to another type.

408 Although we attempted to collect data on all types of atmospheric pollution boundary layer structures in the Beijing area,  
409 there are still certain data samples that were not collected. These data can also explain the pollution characteristics associated  
410 with the four heavy pollution boundary layers from other factors, such as PM<sub>2.5</sub> composition data. We also speculate that  
411 there is feedback between aerosols and the boundary layer, which was not examined in this study. Although there have been  
412 numerous studies on atmospheric pollutant transport, there are few studies on 3-D pollutant transportation, which will be the  
413 focus of our future investigations.

414  
415 *Data availability.* All the data are available upon request via email: xjzhao@ium.cn.

416 *Competing interests.* The authors declare that they have no conflict of interest.

417 *Acknowledgements.* This study is supported by the National Natural Science Foundation of China(41305130), Beijing Major  
418 Science and Technology Project (Z181100005418014), the Natural Science Foundation of Beijing Municipality (8161004)  
419 and the National Natural Science Foundation of China(41975004).

420

421 **References**

- 422 Cai, W. J., Li, K., Liao, H., Wang, H. J., and Wu, L. X.: Weather conditions conducive to Beijing severe haze more frequent  
423 under climate change, *Nat. Clim. Chang.*, 7, 257-262, <http://doi.org/10.1038/nclimate3249>, 2017.
- 424 Chamorro, L. P., and Porte-Agel, F.: Effects of thermal stability and incoming boundary-layer flow characteristics on wind-  
425 turbine wakes: a wind-tunnel study, *Bound.-Layer Meteor.*, 136, 515-533, <http://doi.org/10.1007/s10546-010-9512-1>,  
426 2010.
- 427 Chen, G. T.-J., Jiang, Z., and Wu, M.-C.: Spring heavy rain events in Taiwan during warm episodes and the associated large-  
428 scale conditions, *Monthly Weather Review*, 131, 1173-1188, 2003.
- 429 Chen, H. P., and Wang, H. J.: Haze days in North China and the associated atmospheric circulations based on daily visibility  
430 data from 1960 to 2012, *J. Geophys. Res.-Atmos.*, 120, 5895-5909, <http://doi.org/10.1002/2015jd023225>, 2015.
- 431 D'Elia, I., Bencardino, M., Ciancarella, L., Contaldi, M., and Vialetto, G.: Technical and Non-Technical Measures for air  
432 pollution emission reduction: The integrated assessment of the regional Air Quality Management Plans through the Italian  
433 national model, *Atmos. Environ.*, 43, 6182-6189, <http://doi.org/10.1016/j.atmosenv.2009.09.003>, 2009.
- 434 Ding, A. J., Huang, X., Nie, W., Sun, J. N., Kerminen, V. M., Petaja, T., Su, H., Cheng, Y. F., Yang, X. Q., Wang, M. H.,  
435 Chi, X. G., Wang, J. P., Virkkula, A., Guo, W. D., Yuan, J., Wang, S. Y., Zhang, R. J., Wu, Y. F., Song, Y., Zhu, T.,  
436 Zilitinkevich, S., Kulmala, M., and Fu, C. B.: Enhanced haze pollution by black carbon in megacities in China, *Geophys.*  
437 *Res. Lett.*, 43, 2873-2879, <http://doi.org/10.1002/2016gl067745>, 2016.
- 438 Dockery, D. W., Pope, C. A., 3rd, Xu, X., Spengler, J. D., Ware, J. H., Fay, M. E., Ferris, B. G., Jr., and Speizer, F. E.: An  
439 association between air pollution and mortality in six U.S. cities, *N. Engl. J. Med.*, 329, 1753-1759,  
440 <http://doi.org/10.1056/nejm199312093292401>, 1993.
- 441 He, K. B., Yao, Z. L., and Zhang, Y. Z.: Characteristics of vehicle emissions in China based on portable emission  
442 measurement system, 19th Annual International Emission Inventory Conference “Emissions Inventories-Informing  
443 Emerging Issues”, San Antonio, Texas, 2010.
- 444 Huang, X., Wang, Z. L., and Ding, A. J.: Impact of aerosol-PBL interaction on haze pollution: multiyear observational  
445 evidences in North China, *Geophys. Res. Lett.*, 45, 8596-8603, <http://doi.org/10.1029/2018gl079239>, 2018.
- 446 Inness, A., Benedetti, A., Flemming, J., Huijnen, V., Kaiser, J. W., Parrington, M., and Remy, S.: The ENSO signal in  
447 atmospheric composition fields: emission-driven versus dynamically induced changes, *Atmos. Chem. Phys.*, 15, 9083-  
448 9097, <http://doi.org/10.5194/acp-15-9083-2015>, 2015.
- 449 Lee, Y., Shindell, D. T., Faluvegi, G., and Pinder, R. W.: Potential impact of a US climate policy and air quality regulations  
450 on future air quality and climate change, *Atmos. Chem. Phys.*, 16, 5323-5342, <http://doi.org/10.5194/acp-16-5323-2016>,  
451 2016.

452 Li, J., Du, H. Y., Wang, Z. F., Sun, Y. L., Yang, W. Y., Li, J. J., Tang, X., and Fu, P. Q.: Rapid formation of a severe  
453 regional winter haze episode over a mega-city cluster on the North China Plain, *Environ. Pollut.*, 223, 605-615,  
454 <http://doi.org/10.1016/j.envpol.2017.01.063>, 2017.

455 Li, Q. C., Li, J., Zheng, Z. F., Wang, Y. T., and Yu, M.: Influence of mountain valley breeze and sea land breeze in winter on  
456 distribution of air pollutants in Beijing-Tianjin-Hebei region, *Environmental Science*, 40, 513-524,  
457 <http://doi.org/10.13227/j.hjlx.201803193>, 2019.

458 Liao, Z. H., Sun, J. R., Yao, J. L., Liu, L., Li, H. W., Liu, J., Xie, J. L., Wu, D., and Fan, S. J.: Self-organized classification  
459 of boundary layer meteorology and associated characteristics of air quality in Beijing, *Atmos. Chem. Phys.*, 18, 6771-  
460 6783, <http://doi.org/10.5194/acp-18-6771-2018>, 2018.

461 Markakis, K., Valari, M., Engardt, M., Lacressonniere, G., Vautard, R., and Andersson, C.: Mid-21st century air quality at  
462 the urban scale under the influence of changed climate and emissions - case studies for Paris and Stockholm, *Atmos.*  
463 *Chem. Phys.*, 16, 1877-1894, <http://doi.org/10.5194/acp-16-1877-2016>, 2016.

464 McDonnell, W. F., Nishino-Ishikawa, N., Petersen, F. F., Chen, L. H., and Abbey, D. E.: Relationships of mortality with the  
465 fine and coarse fractions of long-term ambient PM<sub>10</sub> concentrations in nonsmokers, *J. Expo. Anal. Environ. Epidemiol.*,  
466 10, 427-436, <http://doi.org/10.1038/sj.jea.7500095>, 2000.

467 Miao, Y. C., Guo, J. P., Liu, S. H., Liu, H., Li, Z. Q., Zhang, W. C., and Zhai, P. M.: Classification of summertime synoptic  
468 patterns in Beijing and their associations with boundary layer structure affecting aerosol pollution, *Atmos. Chem. Phys.*,  
469 17, 3097-3110, <http://doi.org/10.5194/acp-17-3097-2017>, 2017.

470 Munkel, C., Eresmaa, N., Rasanen, J., and Karppinen, A.: Retrieval of mixing height and dust concentration with lidar  
471 ceilometer, *Bound.-Layer Meteor.*, 124, 117-128, <http://doi.org/10.1007/s10546-006-9103-3>, 2007.

472 Paegle, J. N., and Mo, K. C.: Linkages between summer rainfall variability over South America and sea surface temperature  
473 anomalies, *J. Clim.*, 15, 1389-1407, 2002.

474 Park, J., Basu, S., and Manuel, L.: Large-eddy simulation of stable boundary layer turbulence and estimation of associated  
475 wind turbine loads, *Wind Energy*, 17, 359-384, <http://doi.org/10.1002/we.1580>, 2014.

476 Tang, G., Zhu, X., Hu, B., Xin, J., Wang, L., Munkel, C., Mao, G., and Wang, Y.: Impact of emission controls on air quality  
477 in Beijing during APEC 2014: lidar ceilometer observations, *Atmos. Chem. Phys.*, 15, 12667-12680,  
478 <http://doi.org/10.5194/acp-15-12667-2015>, 2015.

479 Tang, G. Q., Zhang, J. Q., Zhu, X. W., Song, T., Munkel, C., Hu, B., Schafer, K., Liu, Z. R., Zhang, J. K., Wang, L. L., Xin,  
480 J. Y., Suppan, P., and Wang, Y. S.: Mixing layer height and its implications for air pollution over Beijing, China, *Atmos.*  
481 *Chem. Phys.*, 16, 2459-2475, <http://doi.org/10.5194/acp-16-2459-2016>, 2016.

482 Wang, C., An, X., Zhai, S., Hou, Q., and Sun, Z.: Tracking sensitive source areas of different weather pollution types using  
483 GRAPES-CUACE adjoint model, *Atmos. Environ.*, 175, 154-166, <http://doi.org/10.1016/j.atmosenv.2017.11.041>, 2018.

484 Wang, H., Chen, H., and Liu, J.: Arctic sea ice decline intensified haze pollution in Eastern China, *Atmospheric and Oceanic*  
485 *Science Letters*, 8, 1-9, <http://doi.org/10.3878/AOSL20140081>, 2015.

486 Wang, H., Peng, Y., Zhang, X. Y., Liu, H. L., Zhang, M., Che, H. Z., Cheng, Y. L., and Zheng, Y.: Contributions to the  
487 explosive growth of PM<sub>2.5</sub> mass due to aerosol-radiation feedback and decrease in turbulent diffusion during a red alert  
488 heavy haze in Beijing-Tianjin-Hebei, China, *Atmos. Chem. Phys.*, 18, 17717-17733, [http://doi.org/10.5194/acp-18-17717-](http://doi.org/10.5194/acp-18-17717-2018)  
489 [2018](http://doi.org/10.5194/acp-18-17717-2018), 2018.

490 Wang, Z. L., Huang, X., and Ding, A. J.: Dome effect of black carbon and its key influencing factors: a one-dimensional  
491 modelling study, *Atmos. Chem. Phys.*, 18, 2821-2834, <http://doi.org/10.5194/acp-18-2821-2018>, 2018.

492 Wu, J. R., Bei, N. F., Hu, B., Liu, S. X., Zhou, M., Wang, Q. Y., Li, X., Liu, L., Feng, T., Liu, Z. R., Wang, Y. C., Cao, J. J.,  
493 Tie, X. X., Wang, J., Molina, L. T., and Li, G. H.: Aerosol-radiation feedback deteriorates the wintertime haze in the  
494 North China Plain, *Atmos. Chem. Phys.*, 19, 8703-8719, <http://doi.org/10.5194/acp-19-8703-2019>, 2019.

495 Wu, P., Ding, Y. H., and Liu, Y. J.: Atmospheric circulation and dynamic mechanism for persistent haze events in the  
496 Beijing-Tianjin-Hebei region, *Adv. Atmos. Sci.*, 34, 429-440, <http://doi.org/10.1007/s00376-016-6158-z>, 2017.

497 Xu, J. M., Chang, L. Y., Ma, J. H., Mao, Z. C., Chen, L., and Cao, Y.: Objective synoptic weather classification on PM<sub>2.5</sub>  
498 pollution during autumn and winter seasons in Shanghai, *Acta Scientiae Circumstantiae*, 36, 4303-4314,  
499 <http://doi.org/10.13671/j.hjkxxb.2016.0224>, 2016.

500 Zhai, S. X., An, X. Q., Liu, Z., Sun, Z. B., and Hou, Q.: Model assessment of atmospheric pollution control schemes for  
501 critical emission regions, *Atmos. Environ.*, 124, 367-377, <http://doi.org/10.1016/j.atmosenv.2015.08.093>, 2016.

502 Zhang, W., Zhang, Y., Lv, Y., Li, K., and Li, Z.: Observation of atmospheric boundary layer height by ground-based LiDAR  
503 during haze days, *Journal of Remote Sensing*, 17, 981-992, 2013.

504 Zhang, Y., Ding, A. J., Mao, H. T., Nie, W., Zhou, D. R., Liu, L. X., Huang, X., and Fu, C. B.: Impact of synoptic weather  
505 patterns and inter-decadal climate variability on air quality in the North China Plain during 1980-2013, *Atmos. Environ.*,  
506 124, 119-128, <http://doi.org/10.1016/j.atmosenv.2015.05.063>, 2016.

507 Zhao, X., Zhang, X., Xu, X., Xu, J., Meng, W., and Pu, W.: Seasonal and diurnal variations of ambient PM<sub>2.5</sub> concentration  
508 in urban and rural environments in Beijing, *Atmos. Environ.*, 43, 2893-2900,  
509 <http://doi.org/10.1016/j.atmosenv.2009.03.009>, 2009.

510 Zheng, X. Y., Fu, Y. F., Yang, Y. J., and Liu, G. S.: Impact of atmospheric circulations on aerosol distributions in autumn  
511 over eastern China: observational evidence, *Atmos. Chem. Phys.*, 15, 12115-12138, [http://doi.org/10.5194/acp-15-12115-](http://doi.org/10.5194/acp-15-12115-2015)  
512 [2015](http://doi.org/10.5194/acp-15-12115-2015), 2015.

513 Zhong, J. T., Zhang, X. Y., Dong, Y. S., Wang, Y. Q., Liu, C., Wang, J. Z., Zhang, Y. M., and Che, H. C.: Feedback effects  
514 of boundary-layer meteorological factors on cumulative explosive growth of PM<sub>2.5</sub> during winter heavy pollution episodes  
515 in Beijing from 2013 to 2016, *Atmos. Chem. Phys.*, 18, 247-258, <http://doi.org/10.5194/acp-18-247-2018>, 2018.

516 Zhou, D. R., Ding, K., Huang, X., Liu, L. X., Liu, Q., Xu, Z. N., Jiang, F., Fu, C. B., and Ding, A. J.: Transport, mixing and  
517 feedback of dust, biomass burning and anthropogenic pollutants in eastern Asia: a case study, *Atmos. Chem. Phys.*, 18,  
518 16345-16361, <http://doi.org/10.5194/acp-18-16345-2018>, 2018.



519 Zou, Y. F., Wang, Y. H., Zhang, Y. Z., and Koo, J. H.: Arctic sea ice, Eurasia snow, and extreme winter haze in China,  
520 Science Advances, 3, <http://doi.org/10.1126/sciadv.1602751>, 2017.  
521  
522

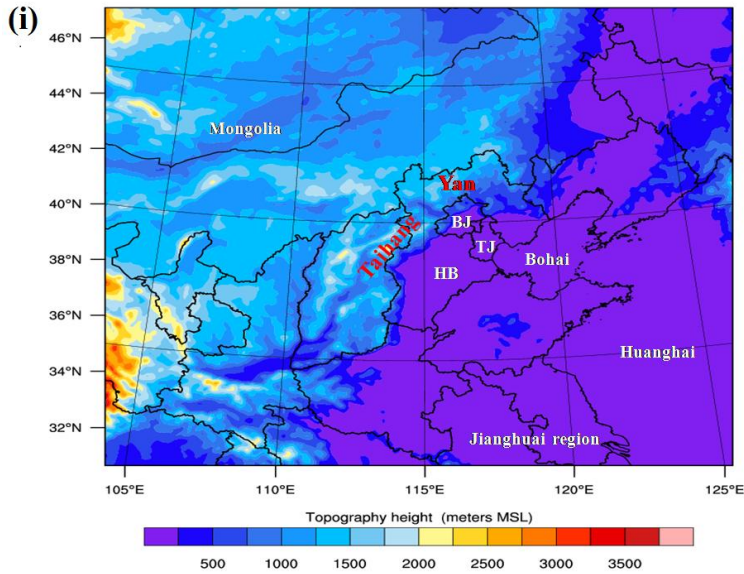
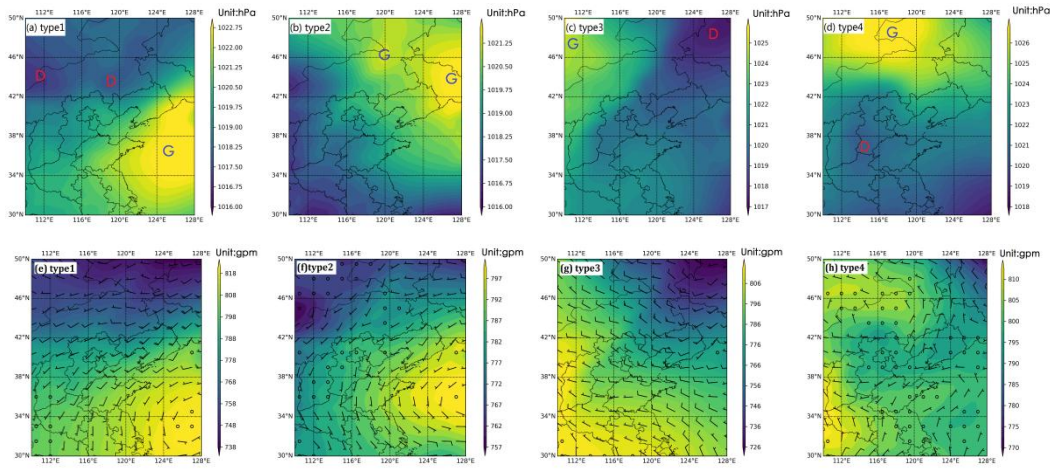
523

524 **Figures and figure captions**

525

526

527



528

529 Figure 1. Sea level pressure (unit: hPa, top), geopotential height of 925hPa(unit: gpm, bottom), wind field (wind direction

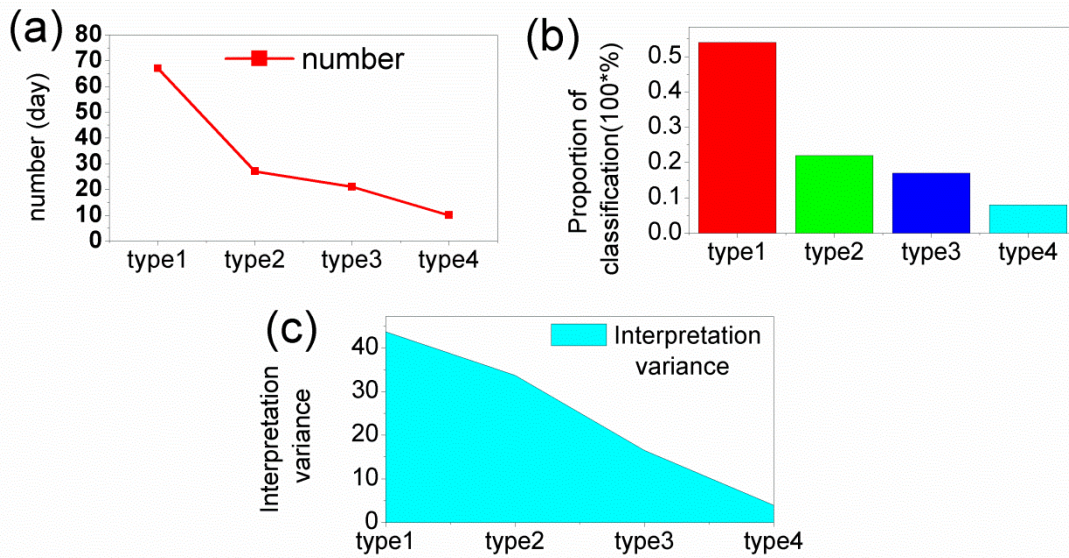
530 bar)for the four heavy pollution weather types in the Beijing area: (a and e) type1, (b and f) type2, (c and g) type3, and (d

531 and h) type4.BJ,TJ and HB represent Beijing, Tianjin and Hebei. Yan and Taihang represent Yan and Taihang mountains.

532

533

534

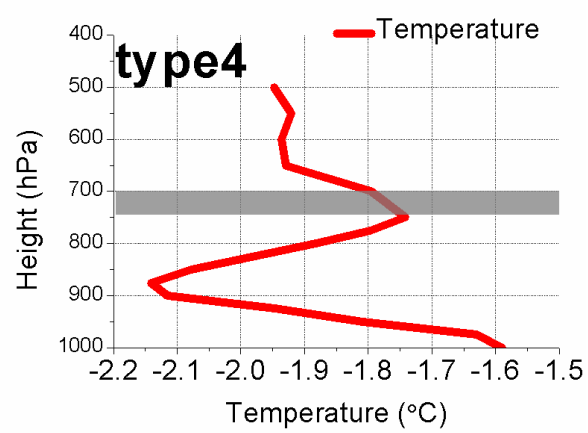
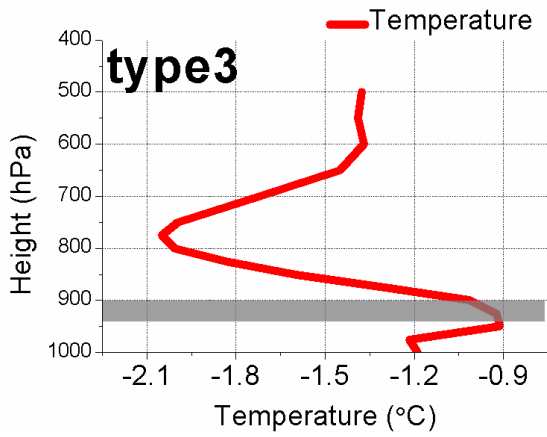
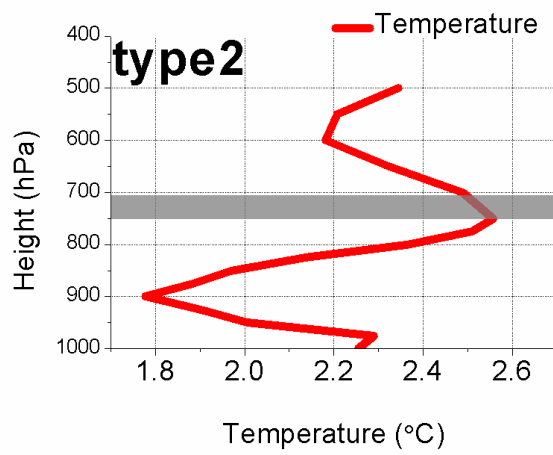
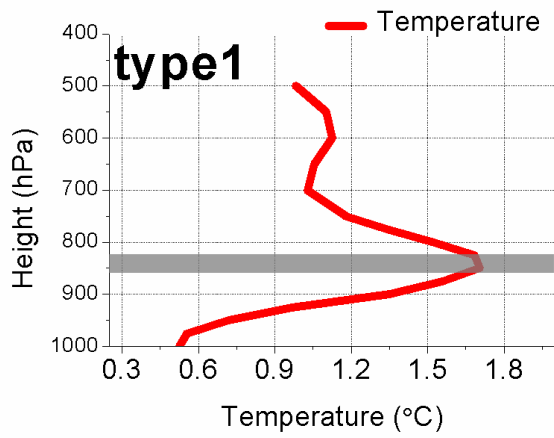


535

536 Figure 2. The four pollution weather types as a function of their (a) number of samples, (b) proportion with respect to the total

537 number of samples, and (c) interpretation variance.

538



539

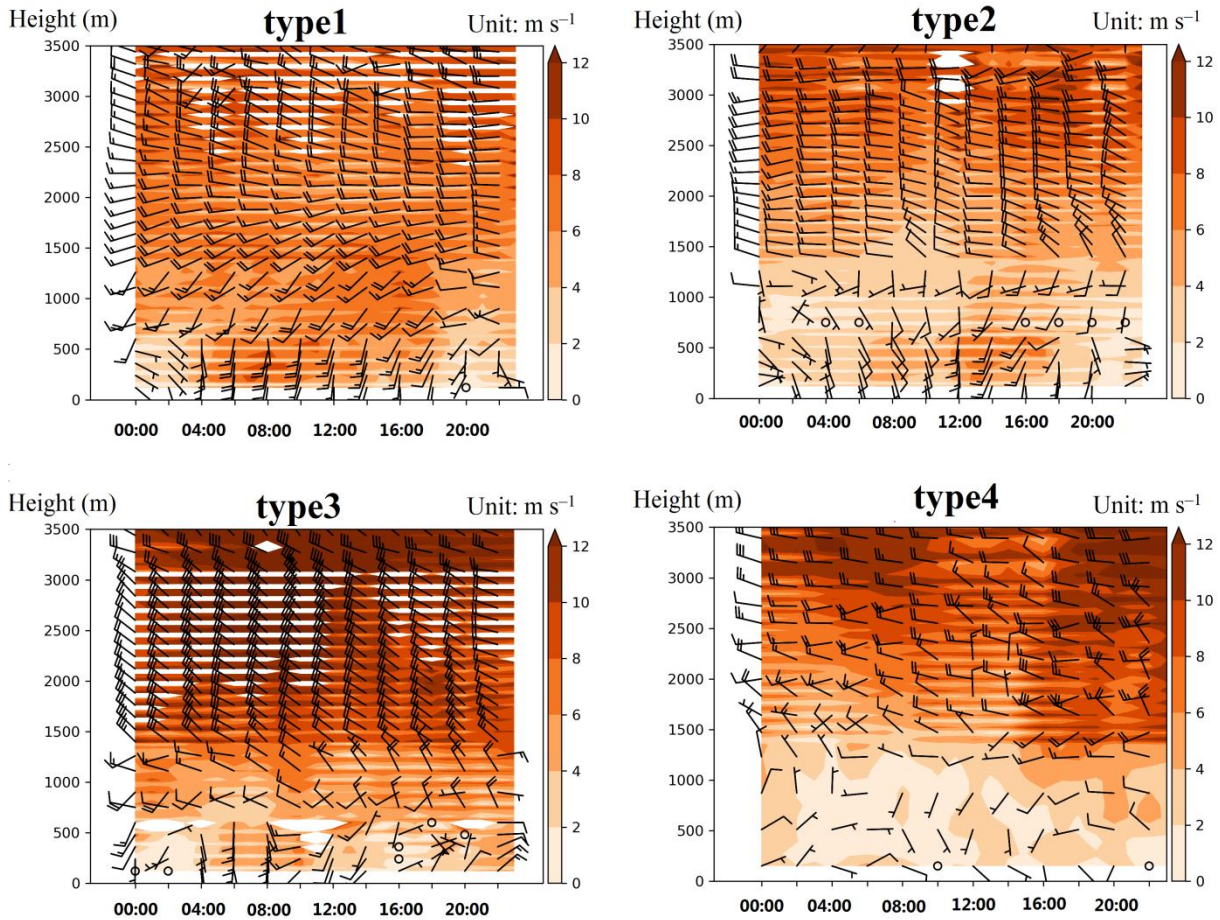
540

541 Fig. 3 Vertical distribution of temperature in pollution boundary layer of four types in Beijing area .Solid red lines represent  
 542 temperatures at different heights. Gray shade represents the top of the inversion layer.

543

544

545



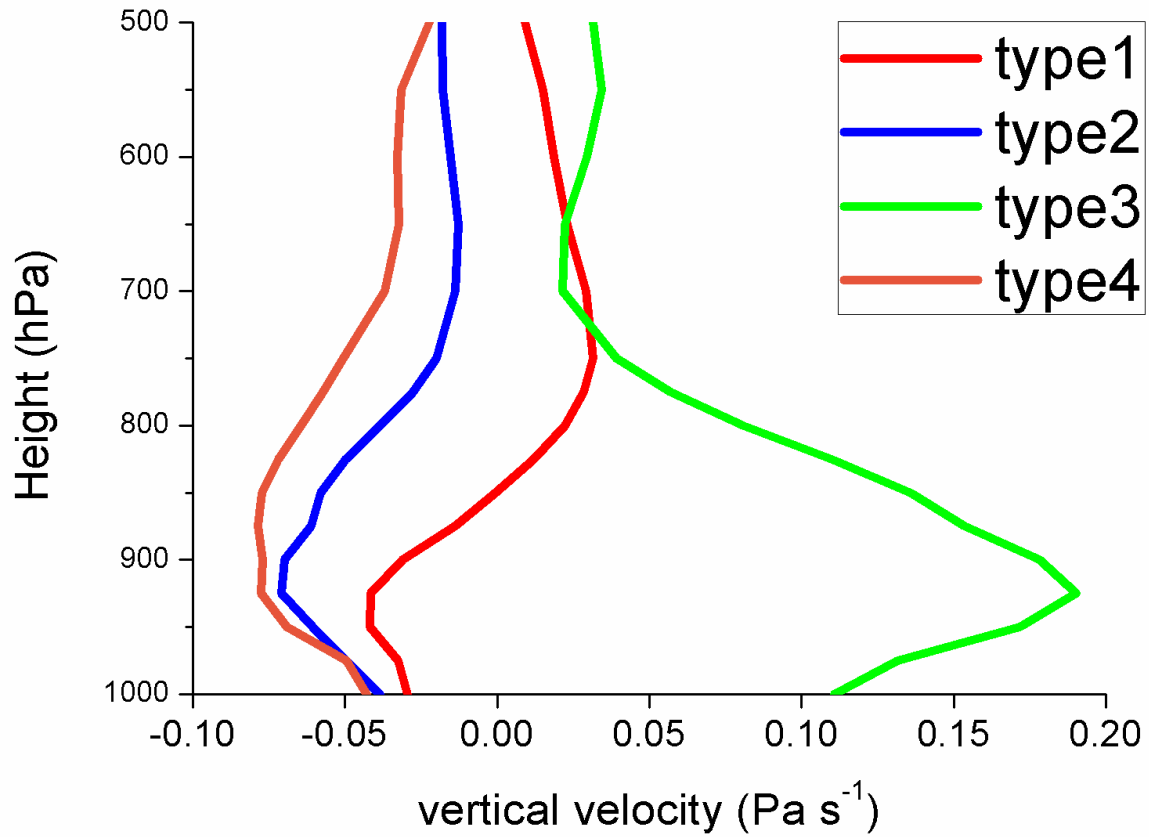
546

547 Figure 4. The mean wind field characteristics of the four pollution weather types in the Beijing area (varying colors, based on  
548 the color bar to the right of each panel, represent the wind speed in  $\text{m s}^{-1}$ ; the x-axis is in Beijing time from 00:00 to 23:00;  
549 the y-axis is the height in m).

550

551

552



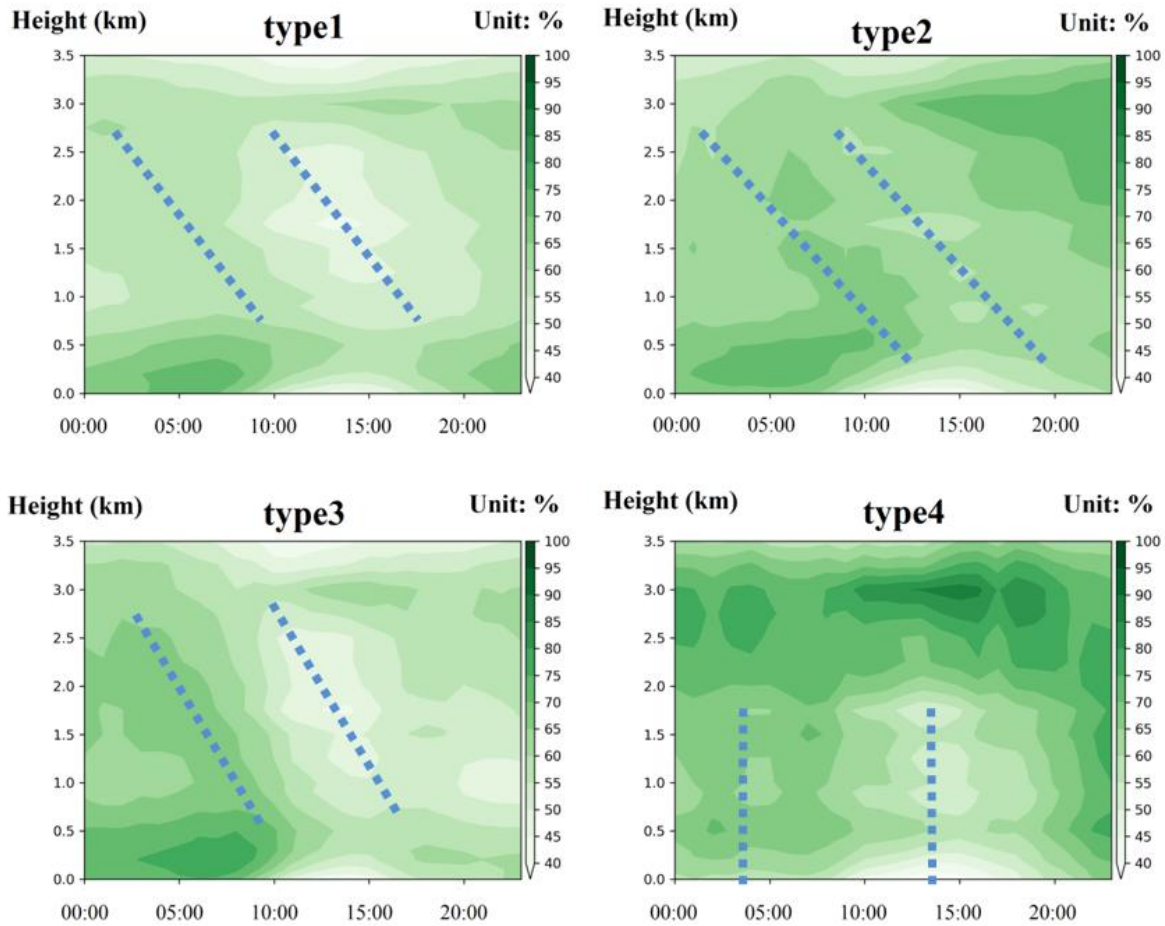
553

554 Figure 5. The vertical speed profiles in the four pollution weather types (type1: red, type2: blue, type3: green, and type4: red)  
555 in the Beijing area. The negative values represent ascending motion while positive values represent descending motion under  
556 the P coordinate (unit: Pa s<sup>-1</sup>).

557

558

559



560

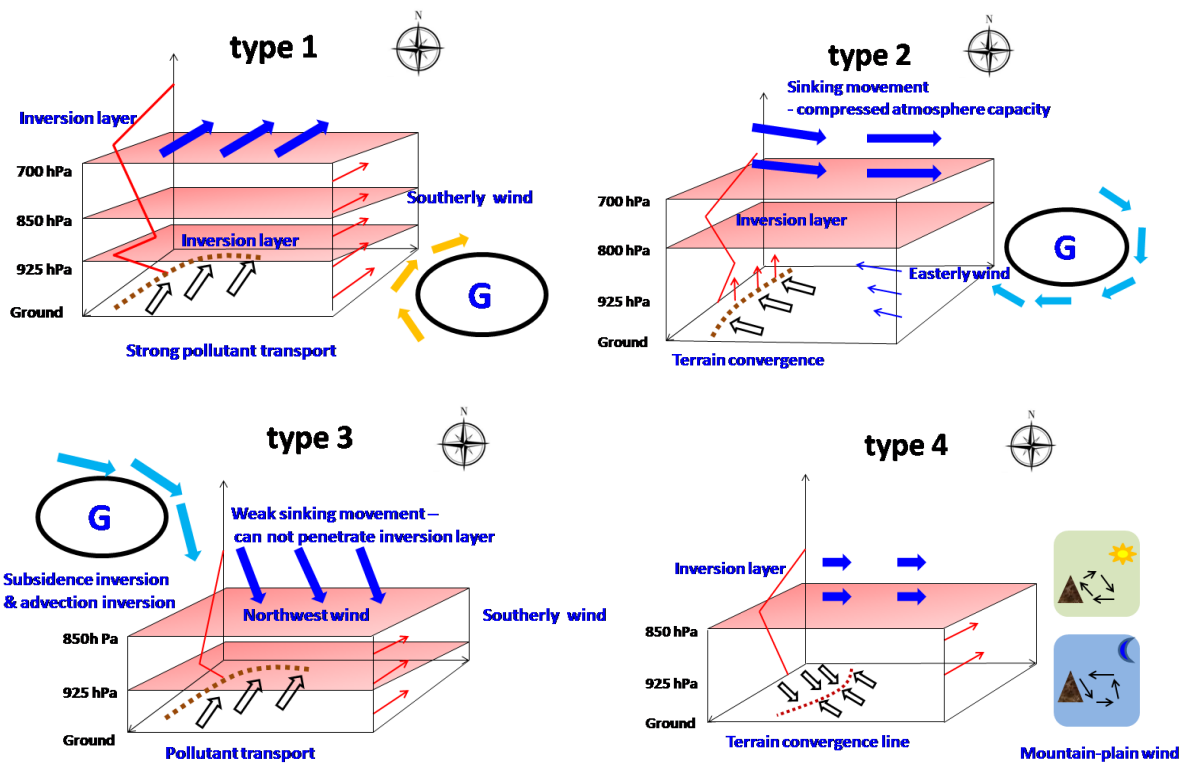
561 Figure. 6 Average characteristics of the relative humidity field in the boundary layer under four pollution types in Beijing  
562 area (shadow represents relative humidity, unit:%; x-axis is Beijing time, from 00:00 to 23:00; y-axis is height, unit: km).

563

564

565

566



567

568

569

570 Figure 7.A thermodynamic and dynamic structure conceptual model of the pollution boundary layer for the four types of  
 571 weather in the Beijing area. Arrows represent wind directions at different heights. Hollow arrow represents the ground  
 572 horizontal wind field, thin red and blue arrows represent wind fields at different heights, and thick blue arrow represents the  
 573 upper wind field. The dark red dots represent ground convergence lines, including 1) convergence between wind fields and 2)  
 574 convergence between wind fields and topography. Solid red line is temperature. The Beijing area is located within the  
 575 lowest rectangle, and the small figure in type4 represents mountain–plain winds with a daily cycle

576

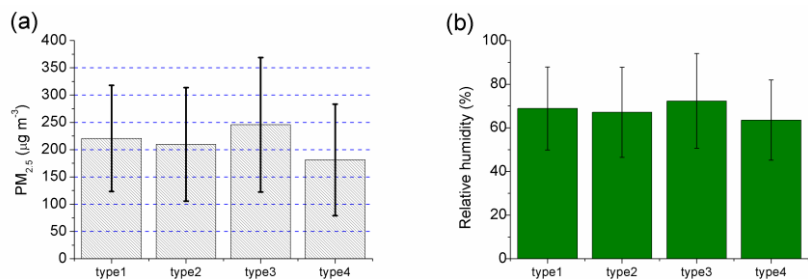
577

578

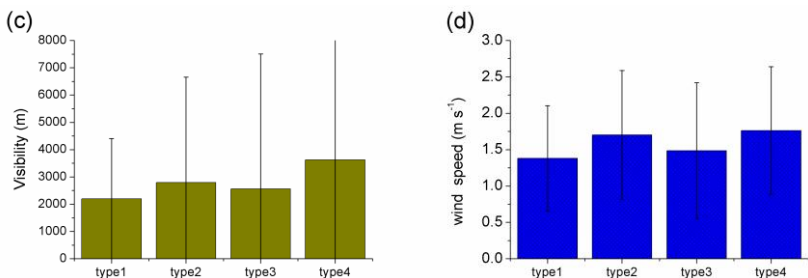


579

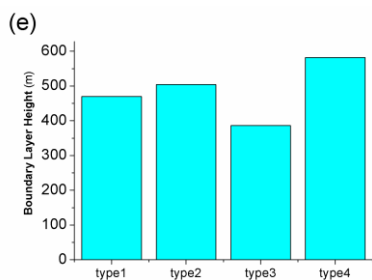
580



581



582



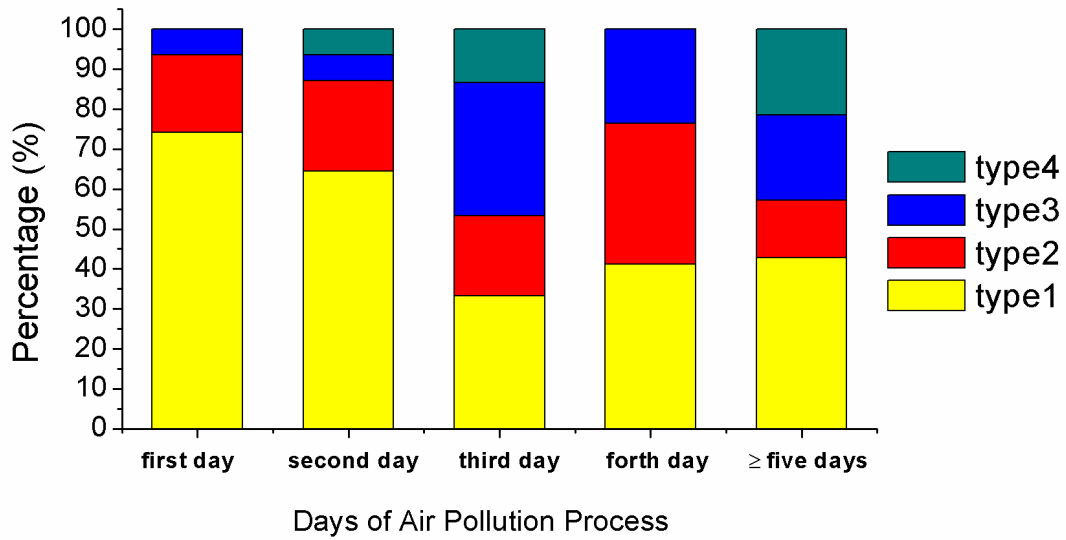
583

584 Figure 8. The four pollution weather types in Beijing area: (a) average daily PM<sub>2.5</sub> concentration at 12 state-controlled  
585 stations (unit:  $\mu\text{g m}^{-3}$ ), (b) average daily relative humidity at the Beijing Observatory (unit: %), (c) average daily visibility at  
586 the Beijing Observatory (unit: m), (d) average daily wind speed at the Beijing Observatory ( $\text{m s}^{-1}$ ), and (e) the boundary  
587 layer height from the tower station at the Institute of Atmospheric Physics, Chinese Academy of Sciences (unit: m).

588

589

590



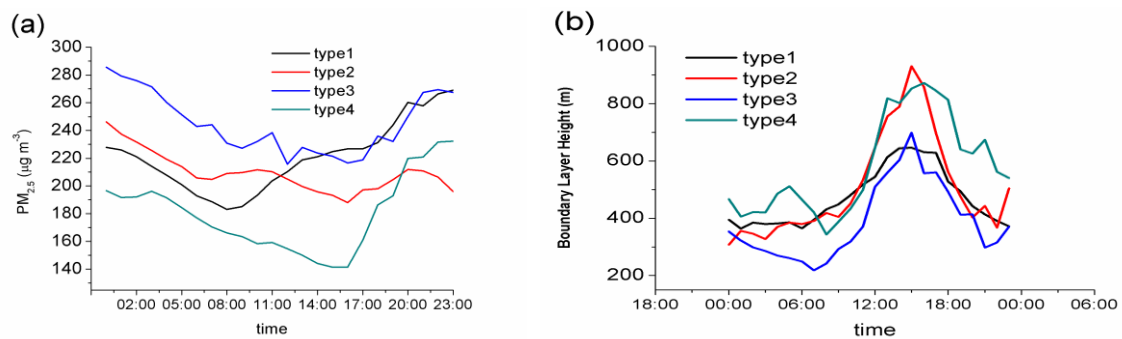
591

592 Figure 9. Time distribution of the four pollution weather types (yellow, red, blue, and green represent type1,type2,type3, and  
593 type4, respectively) during pollution events in the Beijing area.

594

595

596



597

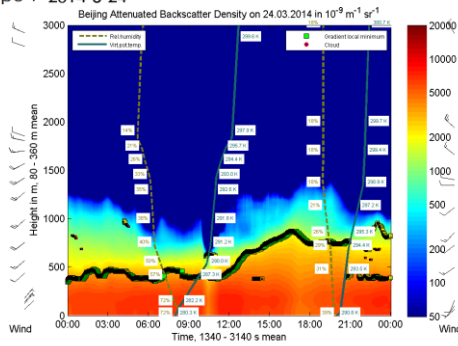
598 Figure 10. Diurnal variation characteristics of the (a) PM<sub>2.5</sub> concentration (μg m<sup>-3</sup>) and (b) boundary layer height (m) under  
599 the four pollution weather types in the Beijing area (x-axis: 00:00–23:00Beijing time).

600

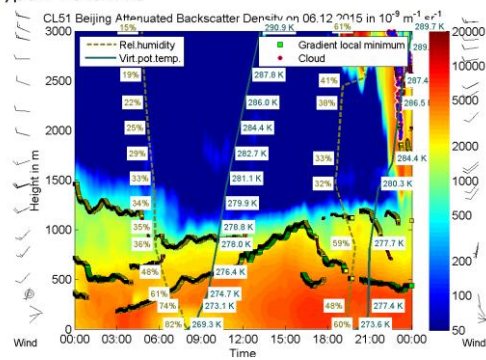
601

602

Type 1 2014-3-24

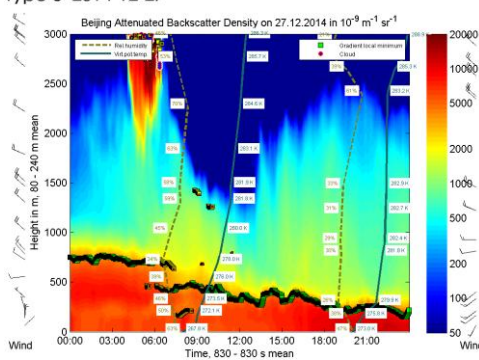


Type 2 2015-12-6

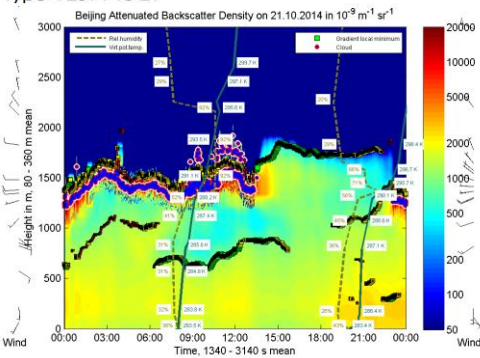


603

Type 3 2014-12-27



Type 4 2014-10-21

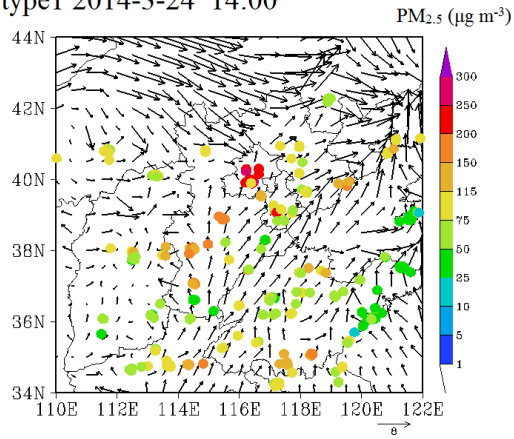


604

605 Figure 11. Aerosol backscattering intensity of the four pollution weather types in the Beijing area and the vertical structure  
606 of meteorological elements at the Beijing Observatory station (y-axis is height in m and the x-axis is Beijing time from  
607 00:00–23:00).

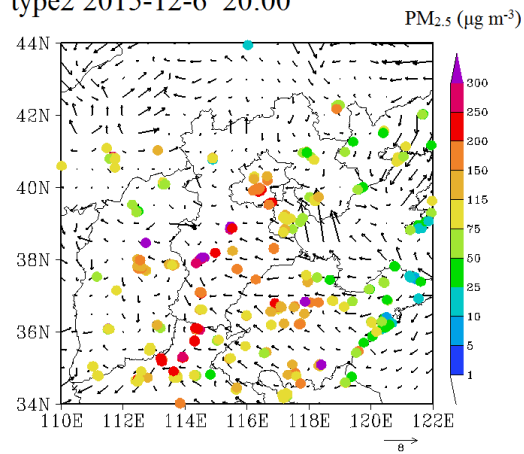
608

type1 2014-3-24 14:00

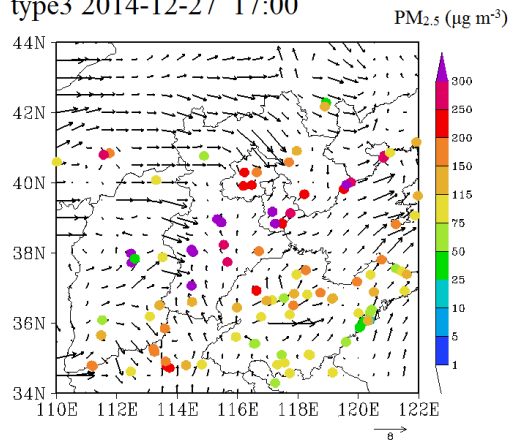


610

type2 2015-12-6 20:00

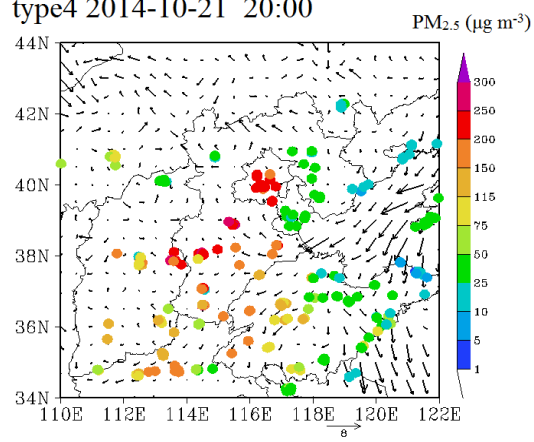


type3 2014-12-27 17:00



611

type4 2014-10-21 20:00



612 Figure 12.  $PM_{2.5}$  concentrations and surface wind fields under the four pollution weather types in the  
 613 North China. Solid circle represents the air pollutant monitoring stations, different colors represent different levels of  
 614 pollution.

615

616